FLOW IN NATURAL AND DYNAMIC AIRWAY GEOMETRIES

Eike Hylla, Octavian Frederich and Frank Thiele
Institute of Fluid Mechanics and Engineering Acoustics
Berlin University of Technology
Müller-Breslau-Str. 8, 10623 Berlin, Germany
e-mail: eike.hylla@cfd.tu-berlin.de

ABSTRACT

In this paper numerical flow predictions within natural airway geometries are presented. The simulations are enabled using an Immersed Boundary approach, which is briefly described. The focus is set on analysing and discussing the flow physics in dynamic as well as in static healthy and injured porcine airways. The results show that the surface deformation has a significant influence on the flow phenomena. Due to negligible geometrical changes of the injured airways, only minor differences of the flow field could be observed, while comparing the results with the healthy airways.

INTRODUCTION AND OBJECTIVES

Understanding the flow physics in the upper airways is an important subject e.g. when optimising the situation for artificially ventilated patients. To achieve that numerical simulations are an essential method to investigate the different physical effects. To gain reliable results realistic airway geometries and boundary conditions are important. Previously the flow in a static human lung and a Weibel lung model (Weibel, 1963) have already been studied and used for method validation (Frederich et al., 2010). Other groups also investigated the flow phenomena in animal, human or models of the lung (Nowak et al., 2003; Kabilan et al., 2007 or Kleinstreuer et al. 2010), but none of these works considered the motion and deformation of the airways, enforced by the diaphragm. Experiments with Computed Tomography (CT) are a common way to capture dynamic in-vivo airway geometries. To take into account the motion of the bronchial tree, a temporal description of the airways is required, which can be gained by a sequence of CT scans during a breathing cycle. As the level of contamination during the repeating CT scans is too high for humans a pork, with a lung geometry similar to those of a human, is used for the investigations. The CT experiments and the segmentation process requires an cooperation with radiologists and experts in medical image processing. The automated and well established workflow is presented in detail by Frederich et al. (2009). In the following sections the numerical methods are presented which enable the flow simulations in complex and moving geometries.

The investigations are split into two parts: The first one deals with the airflow in a dynamic bronchial tree. In this case the dynamics of the bronchial tree (mainly determined by the vertical deformations) is captured by a time resolved CT. In the second part the flow within static healthy and damaged configurations are compared. The artificial injury (Karmrodt et al., 2006) is caused by a treatment (called *lavage*) with liquid acid. Lavage procedures in medical animal experiments are a common way to model the injury of an acute respiratory distress syndrome (ARDS).

WORKFLOW AND DATA ACQUISITION

Computed Tomography and methods of image segmentation (Gergel et al., 2009; Wolber et al., 2008) are utilised to capture the shape and the motion of the porcine bronchial trees, representative for human airways. The important parameters (Reynolds numbers, boundary conditions, etc.) are predefined by the in vivo medical experiments (Zaporozhan et al., 2006). A self-developed flow solver on the basis of the Immersed Boundary (IB-) method is engaged to simulate the respiratory airflow. Finally the results are analysed by both: engineers and physicians.

NUMERICAL METHODOLOGY

The following investigations are based on the three-dimensional, incompressible Navier-Stokes equations (1) and the law of mass conservation for the incompressible case (2):

$$\frac{\partial \vec{u}}{\partial t} + (\vec{u} \cdot \nabla)\,\vec{u} + \frac{1}{\rho}\nabla p - \nu\,\nabla^2 \vec{u} = 0, \tag{1}$$

$$\nabla \cdot \vec{u} = 0, \tag{2}$$

where $\vec{u}$, p, ρ, ν and t are the velocities, pressure, density, kinematic viscosity and time. The employed flow solver (Hylla et al., 2010) applies a Finite-Volume discretisation of second order accuracy in space and time. The flow variables are calculated successively using the SIMPLE algorithm coupling pressure and velocity fields. A non-body conformal Cartesian discretisation is used in which the boundary conditions are imposed by the IB method (Mittal and Iaccarino, 2005).

Immersed Boundary Approach The capabilities of body conformal discretisations are limited, when it is necessary to represent highly complex and/or moving geometries. The IB method is an approach, which is well suited for these applications (Tseng and Ferziger, 2003). It utilises two grids (fig. 1): a Cartesian computational grid Ω and a surface grid Γ_b representing the boundaries of the fluid region Ω_f. This allows the flow simulation on an automatically generated

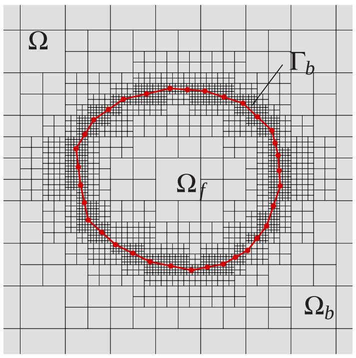

Figure 1. Principle of the IB method: isotropically refined computational grid $\Omega = \Omega_b + \Omega_f$; immersed surface grid Γ_b; non-fluid region Ω_b and fluid region Ω_f.

Cartesian grid, whereas the boundary conditions are imposed at the *immersed* surface mesh. By replacing the surface during the simulation it is possible to realise moving geometries. There are different ways of imposing the boundary conditions in a IB method. The current implementation is based on so called *ghost-cells*. These are cells of the computational domain lying outside but adjacent to the boundary. The flow variables in the ghost-cells are modified in order to fulfil the boundary condition at the IB surface. To distinguish between fluid (Ω_f) and non-fluid (Ω_b) regions, an identification and marking preprocess has to be performed whenever the surface grid changes.
The surface velocity u_{ib} can be approximated with a central difference scheme:

$$\vec{u}_{\mathrm{ib}} = \frac{\mathrm{d}\vec{x}}{\mathrm{d}t} \approx \frac{\vec{x}(t+\Delta t) - \vec{x}(t-\Delta t)}{2\,\Delta t} \ , \tag{3}$$

where $\vec{x}$ is the vector to the points of the surface grid.

INVESTIGATIONS

In this paper two different investigations are discussed. The first part covers the simulation of the air flow in naturally moving porcine airways. The main objectives are to get an insight into the flow physics under normal breathing conditions and to identify differences to the airflow in static geometries. In the second part the flow physics between a healthy and an artificially damaged geometry are examined. The medical experiment (Karmrodt et al., 2006) did not include the dynamics of the bronchial tree and therefore only static configurations are considered.

Dynamic Porcine Airways

After presenting the simulation setup and its parameters in the following section, some selected results are discussed.

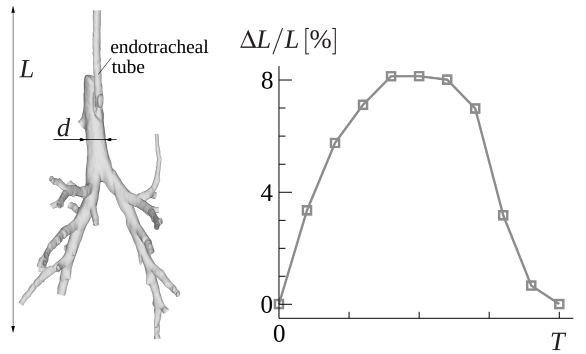

Figure 2. Surface description of the porcine bronchial tree (*left*). Maximum vertical deformations of the surface grid over one breathing cycle, represented by 10 surface configurations (*right*).

Simulation Setup and Parameters Figure 2 *left* displays one of the ten surface configurations which have been gained over one breathing cycle, representing the dynamics of the bronchial tree. As this temporal resolution is too coarse, additional surface configurations are interpolated linearly (see fig. 2 *right*). Finally the complete respiratory cycle is defined by 320 configurations or timesteps respectively. During the animal experiment (Zaporozhan et al., 2006) the anesthetised pork has been mechanically ventilated with an inspiratory to expiratory ratio of 1:2. The segmented data (fig. 2 *left*) contains the endotracheal tube, used for the ventilation. This tube is considered in the following investigations. At the upper end of the endotracheal tube the inlet boundary condition is applied, whereas the 24 trimmed highest level branches are defined as outlet boundary conditions. A prescribed mass flux at both types of boundary conditions is present. The velocities $\vec{u}_i^{\,\mathrm{out}}$ of the $i = 24$ outlets are defined hence that:

$$\sum_{i=1}^{24} A_i^{\mathrm{out}}\, |\vec{u}_i^{\,\mathrm{out}}| = A^{\mathrm{in}}\, |\vec{u}^{\,\mathrm{in}}|. \tag{4}$$

Thus a constant velocity distribution at all outlets is existent. As the respiratory diagram has not been recorded at the experimental stage of the work, it has been reconstructed for the numerical setup: The inspiratory mass flux equals the expiratory: $\dot{m}_{\mathrm{in}} = \dot{m}_{\mathrm{ex}}$. With almost constant cross sections at the outlets the mass flux depends on the absolute velocity magnitude. To modulate the velocities at the boundary conditions (changing inlet to outlet and vice versa), a dimensionless amplification function $\gamma(t)$ can be derived:

$$\gamma(t) = \begin{cases} \gamma_{\mathrm{in}} \sin\left(\frac{3\pi t}{T}\right) & \text{for} \quad 0 < t < T/3 \\ \gamma_{\mathrm{ex}} \sin\left(\frac{3\pi t}{2T} + \frac{\pi}{2}\right) & \text{for} \quad T/3 < t < T. \end{cases} \tag{5}$$

Applying of the law of mass conservation to the amplification function:

$$\int_0^{T/3} \gamma_{\text{in}} \sin\left(\frac{3\pi t}{T}\right) \mathrm{d}t = \int_{T/3}^{T} \gamma_{\text{ex}} \sin\left(\frac{3\pi t}{2T} + \frac{\pi}{2}\right) \mathrm{d}t \qquad (6)$$

leads to an ratio of $\gamma_{\text{in}}/\gamma_{\text{ex}} = 2$. The generic respiratory diagram for one breathing cycle is displayed in figure 3. The

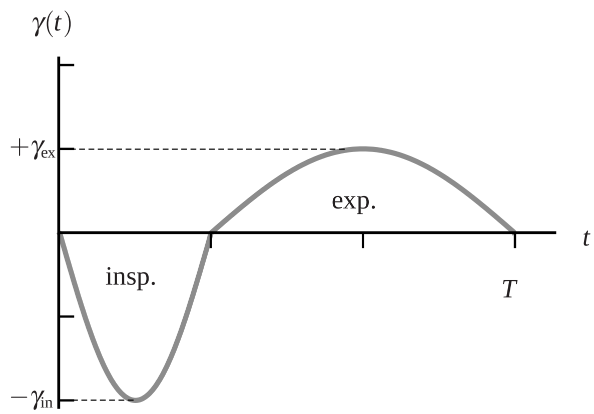

Figure 3. Generic respiratory diagram with an inspiratory to expiratory ratio of 1:2.

Reynolds number at the trachea is $\mathrm{Re}_d = 2000$ according to the experiments. Preliminary investigations (Frederich et al., 2010) have shown, that the flow in the airways can be assumed to be laminar. The computational grid consists of about 2.0 million Cartesian grid cells and the surface mesh covers about 280 000 triangle elements.

Results In the following simulations the inversion of flow direction (inspiration to expiration) and the natural motion of the bronchial tree is considered. The significant influence of the dynamics of the bronchial tree is shown in figure 4. Steady inspiratory flow in a static and a dynamic bronchial tree are compared: The high velocity values are shifted to the rear centre of the trachea and the recirculation region r_1 decreases. In the left daughter branch the recirculation r_2 totally vanishes whereas the velocity profile in the right branch is shifted to the left. Values of the helicity ($H = \vec{u} \cdot (\nabla \times \vec{u})$) can be used to indicate rotational secondary flow motion, whereby the sign defines the direction of the rotation. As shown in figure 5 the rotatory influence during inspiration is more important than during the expiration phase. Depending on the flow direction the bifurcations divide or join the mass fluxes, which is the reason for the different helicity intensities. These counter rotating vortex pairs have also been observed in human airways (Frederich et al., 2010).

Figure 6 depicts the temporal development of velocity components for selected positions. An interpolation of their coordinates in each timestep is necessary due to the motion of the surrounding geometry. As the flow directions in the points usually do not coincide with the coordinate axis (x, y, z) arbitrary contributions of u, v and w appear. At positions close to

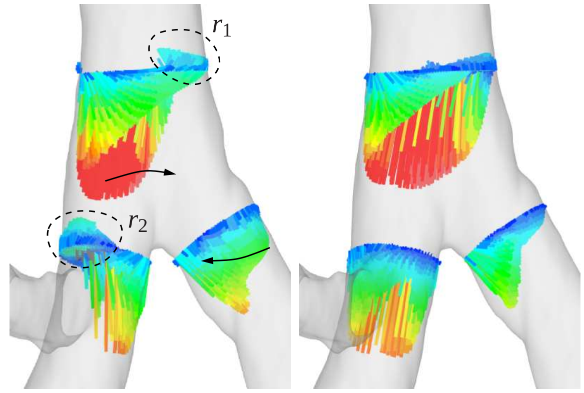

Figure 4. Velocity profiles (colour coded with absolute velocity magnitude) at steady inspiration in the static (*left*) and a dynamic geometry (*right*).

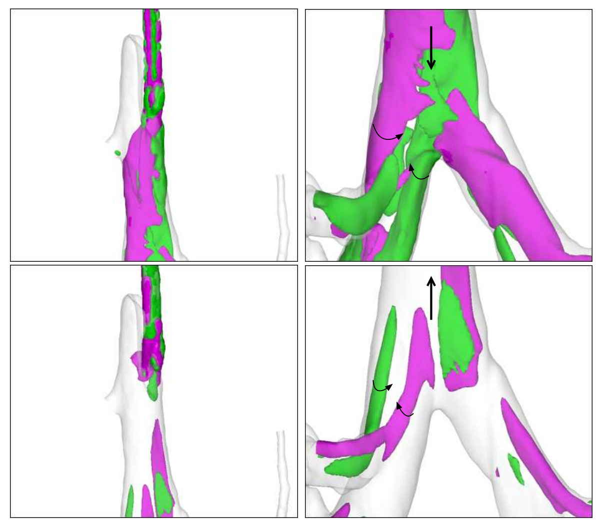

Figure 5. Positive and negative helicity iso surfaces indicating counter rotating secondary flow motion during maximum inspiratory (*upper row*) and maximum expiratory phase (*lower row*).

the in- or outlets, e.g. ① or ⑨, the monitored signal is similar to generic respiratory diagram applied at the boundary conditions. At other positions within the geometry the temporal history clearly differs from the respiratory diagram. The sudden changes and local peaks indicate the existence of secondary flow motion.

Comparison of Healthy and Damaged Airways

Sinclair et al. (2007) reported on a dramatic increase of the dead space (the volume of the airways which does not contribute to the gas exchange) in animal models during mechanical ventilation. To investigate the influence of an increased dead space and an enlarged bronchial tree, simulations within healthy and injured are performed and compared. In the experiment of Sinclair et al. rats have been ventilated with different tidal volumes under a positive end-expiratory pressure (PEEP). The data used in the current work originates from an

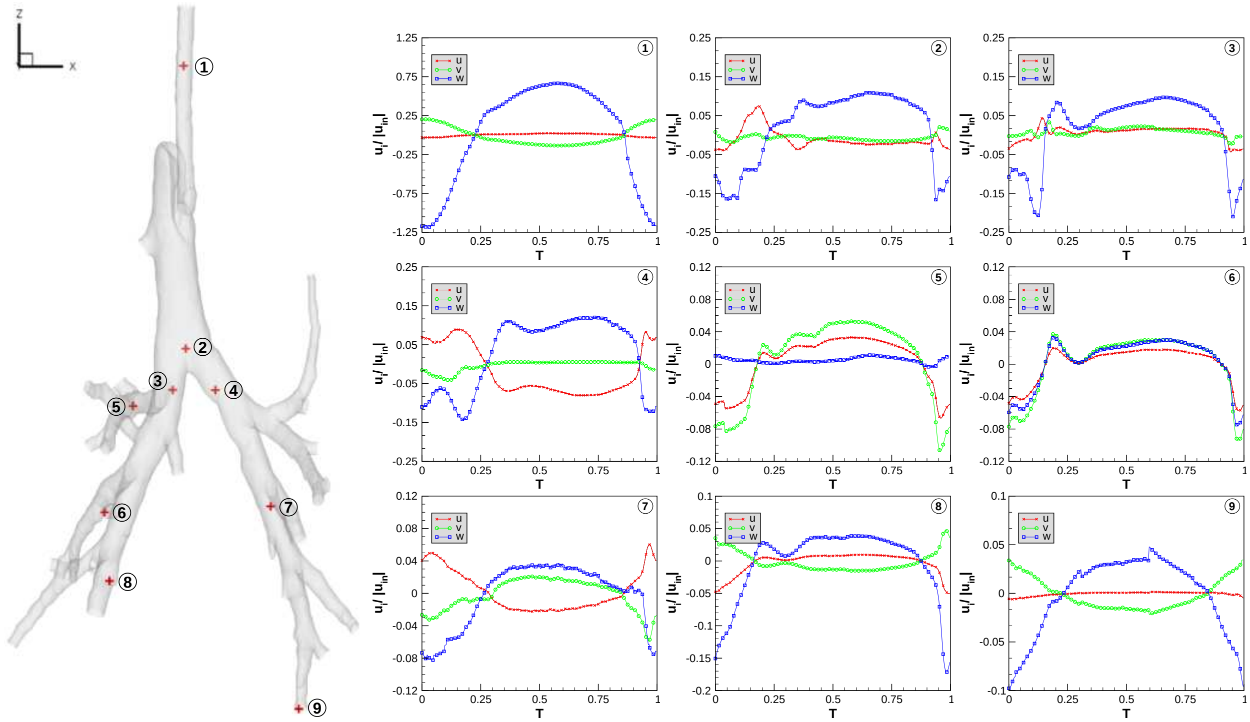

Figure 6. Velocity components over one breathing cycle for 9 different points within the dynamic geometry.

experiment with porcine airways treated by a lavage procedure (Karmrodt et al., 2006). Unfortunately the effect of geometrical change was much smaller than expected (see fig. 7).

Simulation Setup and Parameters The two surface grids (about 274 000 triangle elements) are shown in figure 7. Optimal conditions for the comparison are obtained by exactly putting the two geometries in the same position. Furthermore they are trimmed at identical positions. The trimming is necessary to remove regions of false segmentation or unrealistic shape and to gain well defined surfaces to apply the in- and outlet boundary conditions. To determine the cutting positions, points on the skeleton lines of the geometries are chosen manually (see fig. 8). The measured volumetric difference from healthy to damaged configuration is approximately $\mathrm{d}V = 5\%$. Despite the very small variances between the two cases, the inspiratory and expiratory flow have been simulated. The corresponding computational grid consists of about 2.2 million Cartesian cells. The Reynolds number is $\mathrm{Re}_d = 2000$ with respect to the diameter of the trachea and the mean inlet velocity. No endotracheal tube is present in these cases and the trimmed trachea is predefined with an uniform inlet profile. Although this is not an realistic inlet condition it is sufficient for the comparison. The faces of the 25 trimmed branches are defined as outlet boundary conditions. Again a laminar flow regime is considered.

Results For these two configurations the total area of all outlet branches is smaller than the inlet area. Due to mass conservation, the fluid accelerates behind the first bifurcations. As expected, the flow physics for the healthy and injured airways are almost identical. Figure 9 shows little differences of the velocity distributions for some selected slices. At some branches in the healthy geometry higher velocities appear, which are caused by smaller cross sections. For a more precise comparison, the pressure coefficient c_p along two streamtraces through the left and right main branch are displayed in figure 10. Except the small peak in the left branch of the damaged geometry $(z \approx 0.2)$, the pressure developments coincide with each other. The difference is caused by a local constriction in the injured branch. The analysis also reveals that the pressure drop before the first bifurcation can

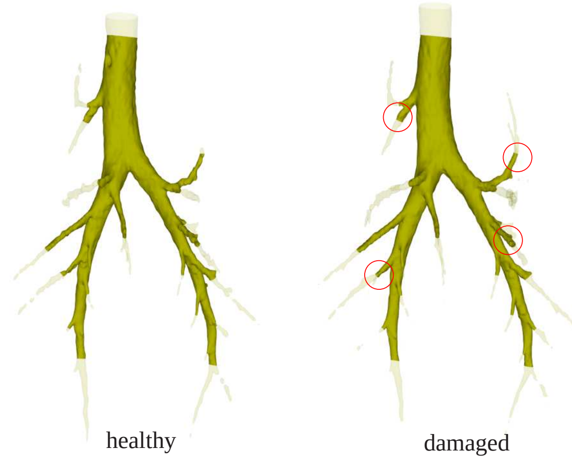

Figure 7. Comparing healthy and damaged airway geometries: minor differences highlighted with red marks. The light colour shows branches which are removed by the trimming process.

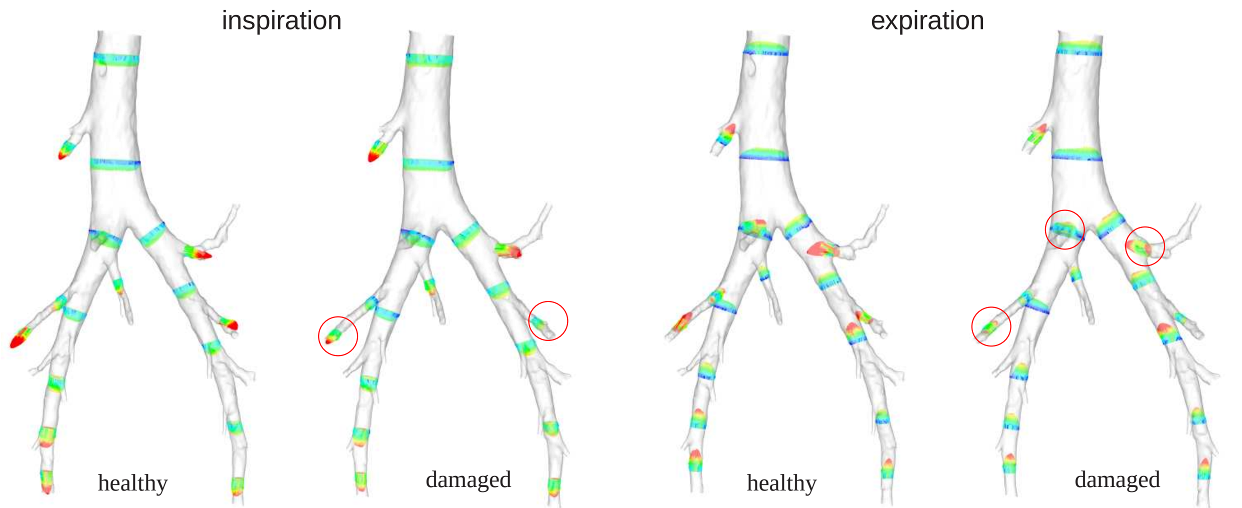

Figure 9. Velocity profiles for the healthy and damaged airway geometry at inspiratory (*left*) and expiratory flow (*right*). Differences highlighted with red marks.

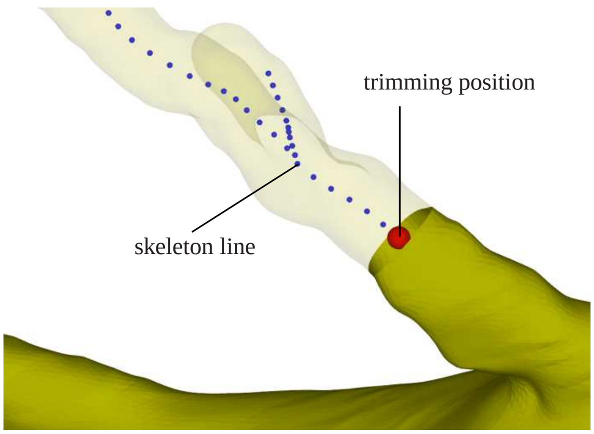

Figure 8. Determining the trimming position, using the skeleton line, generated during the segmentation process.

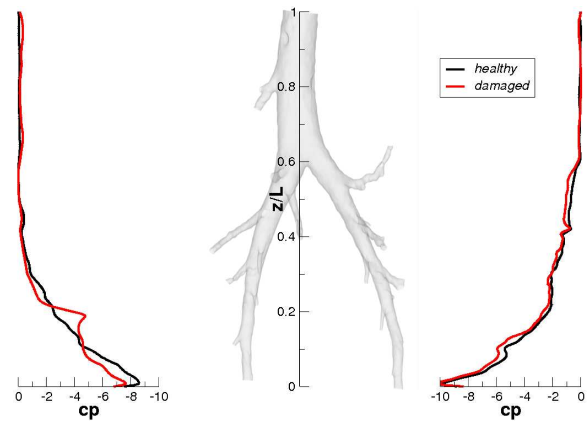

Figure 10. Pressure coefficient along streamtraces through the left and right main bronchi.

be neglected as it rises with decreasing cross sections.
The situation at steady expiration is quite similar to the inspiratory flow. Although the flow direction is inverted, no significant differences between the healthy and damaged bronchial trees can be discovered (compare fig. 9 *right*).

CONCLUSIONS AND OUTLOOK

A numerical approach based on the Immersed Boundary method is presented, which has been successfully applied to the respiratory airflow in porcine airways. The investigations of the flow in moving airway geometries revealed the important influence of the dynamics of the bronchial tree. Local changes of the velocity field can be observed at several points within the bronchial tree. They show a development different from the prescribed respiratory diagram at the in- and outlet boundary conditions, an evidence for the presence of secondary flow motion. The comparison between the flow in a healthy and injured bronchial tree of a pork is unsatisfactory, as the two geometries are almost identical with a very slight increase of the dead space. Therefore no changes of the flow physics have been found, which could have been expected. The increase of the dead space seems to be much more distinct at smaller animals than at larger ones. To gain surface geometries with this characteristic our cooperation partner will perform animal experiments at mechanically ventilated rats. In the near future the results of the numerical studies will be interpreted by medical experts to optimise the process of artificial respiration. Currently the numerical method is enhanced by the implementation of adaptive grids allowing a local solution based refinement or coarsening of the grid. This will improve the spatial resolution where it is necessary and concurrently reduce the computational coasts for further investigations.

ACKNOWLEDGEMENTS

The financial support of the German Research Foundation (DFG) within the scope of the research project "Protective Artificial Respiration" is gratefully acknowledged.

REFERENCES

Weibel, E. R., 1963, "Morphometry of the human lung", Springer, Berlin.

Frederich, O., Amtsfeld, P., Hylla, E., Thiele, F., Puderbach, M., Kauczor, H.-U., Wegner, I. and Meinzer, H.-P., 2010, "Numerical Simulation and Analysis of the Flow in Central Airways", STAB 2008, *Notes on Numerical Fluid Mechanics and Multidisciplinary Design VII*, Vol. 112, pp. 497–504.

Frederich, O., Hylla, E., Amtsfeld, P., Thiele, F., Puderbach, M., Kauczor, H.-U., Wegner, I., and Meinzer, H.-P, 2009, "Numerically Predicted Flow in Central Airways: Modelling, Simulation and Initial Analysis", *in: Proceedings of 6th Int. Symposium Turbulence and Shear Flow Phenomena*, Seoul.

Nowak, N., Kakade, P. P. and Annapragada, A. V., 2003, "Computational Fluid Dynamics Simulation of Airflow and Aerosol Deposition in Human Lungs", *Annals of Biomedical Engineering*, Vol. 31, pp. 374–390.

Kabilan, S., Lin, C.-L. and Hoffman, E. A., 2007, "Characteristics of airflow in a CT-based ovine lung: a numerical study", *Journal of Applied Physiology*, Vol. 102, pp. 1469–1482.

Kleinstreuer, C. and Zhan, Z., 2010, "Airflow and Particle Transport in the Human Respiratory System", *Annual Review of Fluid Mechanics*, Vol. 42, pp. 301-334.

Gergel, I., Wegner, I., Tetzlaff, R., and Meinzer, H.-P., 2009, "Zweistufige Segmentierung des Tracheobronchialbaums mittels iterativen adaptiven Bereichswachstumsverfahren", *Bildverarbeitung für die Medizin*, pp. 56–60.

Wolber, P., Wegner, I., Heimann, T., Wolf, I. and Meinzer, H.-P., 2008, "Tracking und Segmentierung baumförmiger, tubulärer Strukturen mit einem hybriden Verfahren", *Bildverarbeitung für die Medizin*, pp. 242–246.

Zaporozhan, J., Ley, S., Unterhinninghofen, R., Saito, Y., Fabel-Schulte, M., Keller, S., Szabo, G. and Kauczor, H.-U., 2006, "Free-breathing threedimensional computed tomography of the lung using prospective respiratory gating: charge-coupled device camera and laser sensor device in an animal experiment", *Investigative Radiology*, Vol. 41, pp. 468–475.

Peskin, C. S., 2002, "The immersed boundary method", *Acta Numerica*, Cambridge University Press, pp. 479–512.

Hylla, E., Frederich, O., Mauß, J. and Thiele, F., 2010, "Application of the immersed boundary method for the simulation of incompressible flows in complex and moving geometries", STAB 2008, *In: Notes on Numerical Fluid Mechanics and Multidisciplinary Design VII*, Vol. 112, pp. 135–142.

Mittal, R. and Iaccarino, G, 2005, "Immersed boundary methods", *Annual Review of Fluid Mechanics*, Vol. 37, pp. 239–26.

Tseng,Y.H., Ferziger, J. H., 2003, "A ghost-cell immersed boundary method for flow in complex geometry", *Journal of Computational Physics*, Vol. 192, pp. 593–623.

Karmrodt, J., Beltz, C. Yuan, S., David, M., Heussel, C.-P. and Markstaller, K., 2006, "Quantification of atelectatic lung volumes in two different porcine models of ARDS", British Journal of Anaesthesia, 97(6), pp. 883–895.

Sinclair, S. E., Molthen, R. C., Haworth, S. T., Dawson, C. A. and Water, C. M., 2007, "Airway Strain during Mechanical Ventilation in an Intact Animal Model", *American Journal of Respiratory and Critical Care Medicine*, Vol. 176, pp. 786–794.

Hylla, E., Frederich, O., Thiele, F., Puderbach, M., Ley-Zaporozhan, J., Kauczor, H.-U., Wang, X., Meinzer, H.-P., and Wegner, I., 2011, "Analysis of the Flow in Dynamically Changing Central Airways". *Fundamental Medical and Engineering Investigations on Protective Artificial Respiration*, Vol. 116, pp 33–48.